

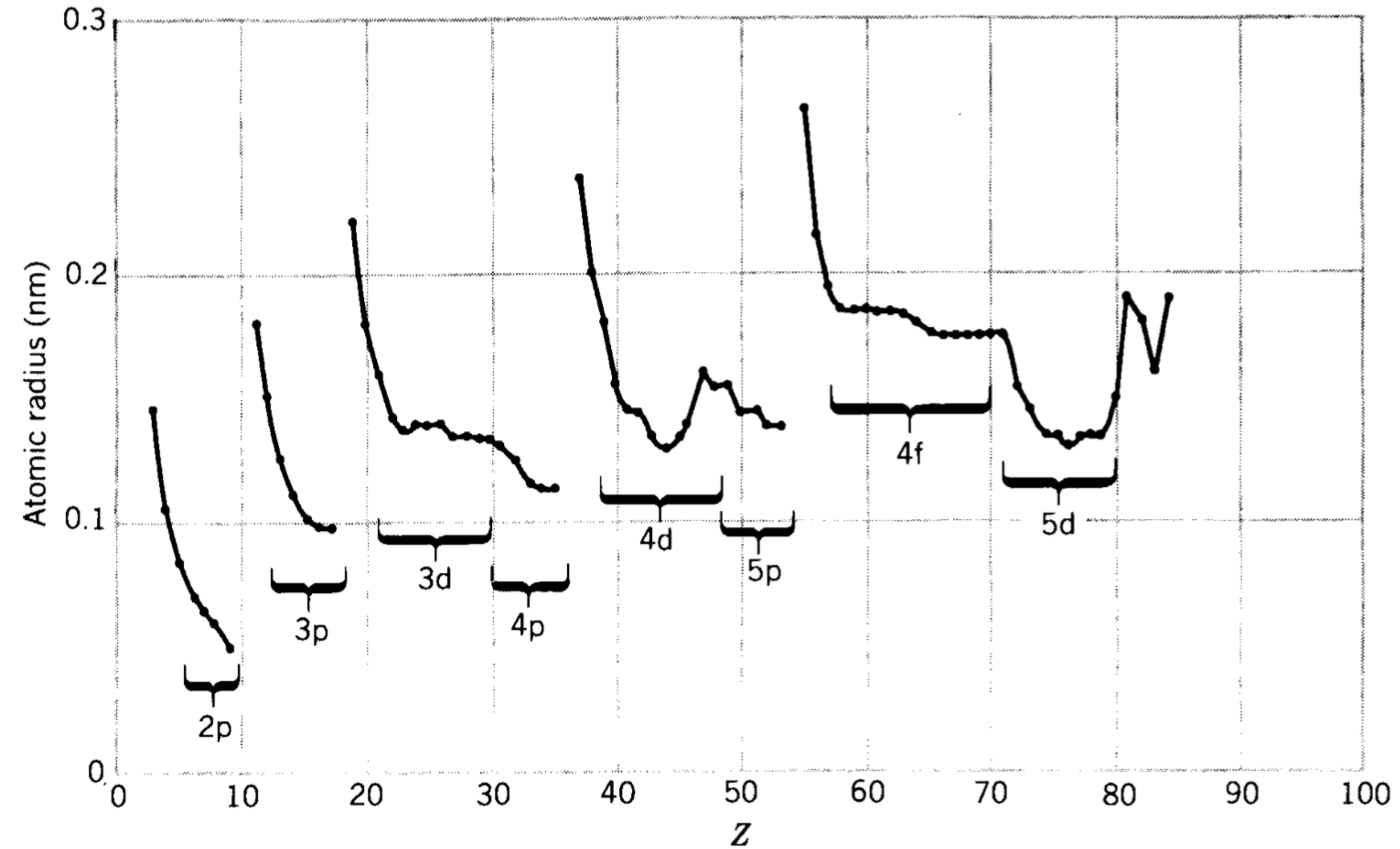
Introduction to Nuclear and Particle Physics

Nuclear models

Helga Dénés 2022 Yachay Tech

hdenes@yachaytech.edu.ec

Atomic shells



atomic shells

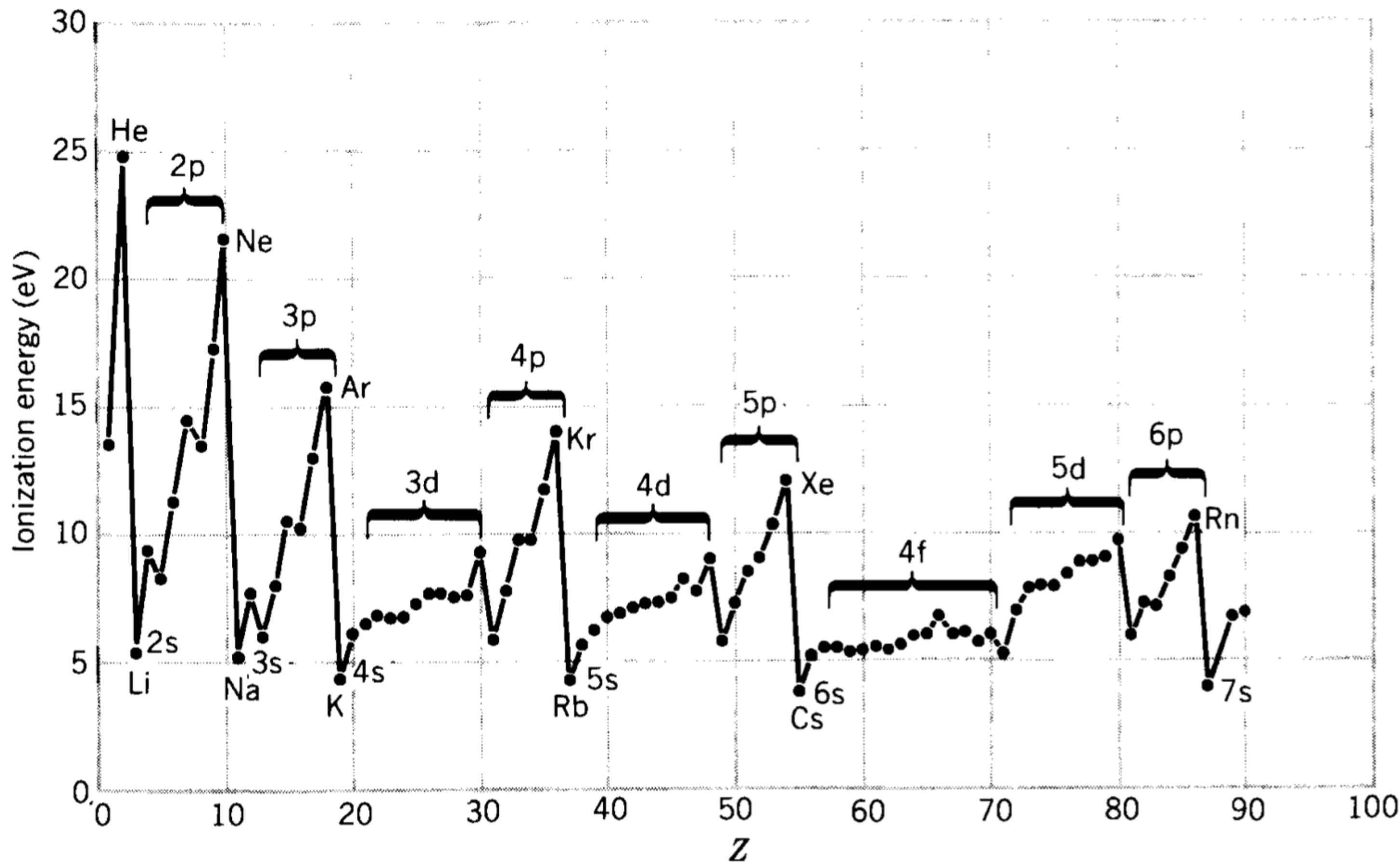


Figure 5.1 Atomic radius (top) and ionization energy (bottom) of the elements. The smooth variations in these properties correspond to the gradual filling of an atomic shell, and the sudden jumps show transitions to the next shell.

Shell model

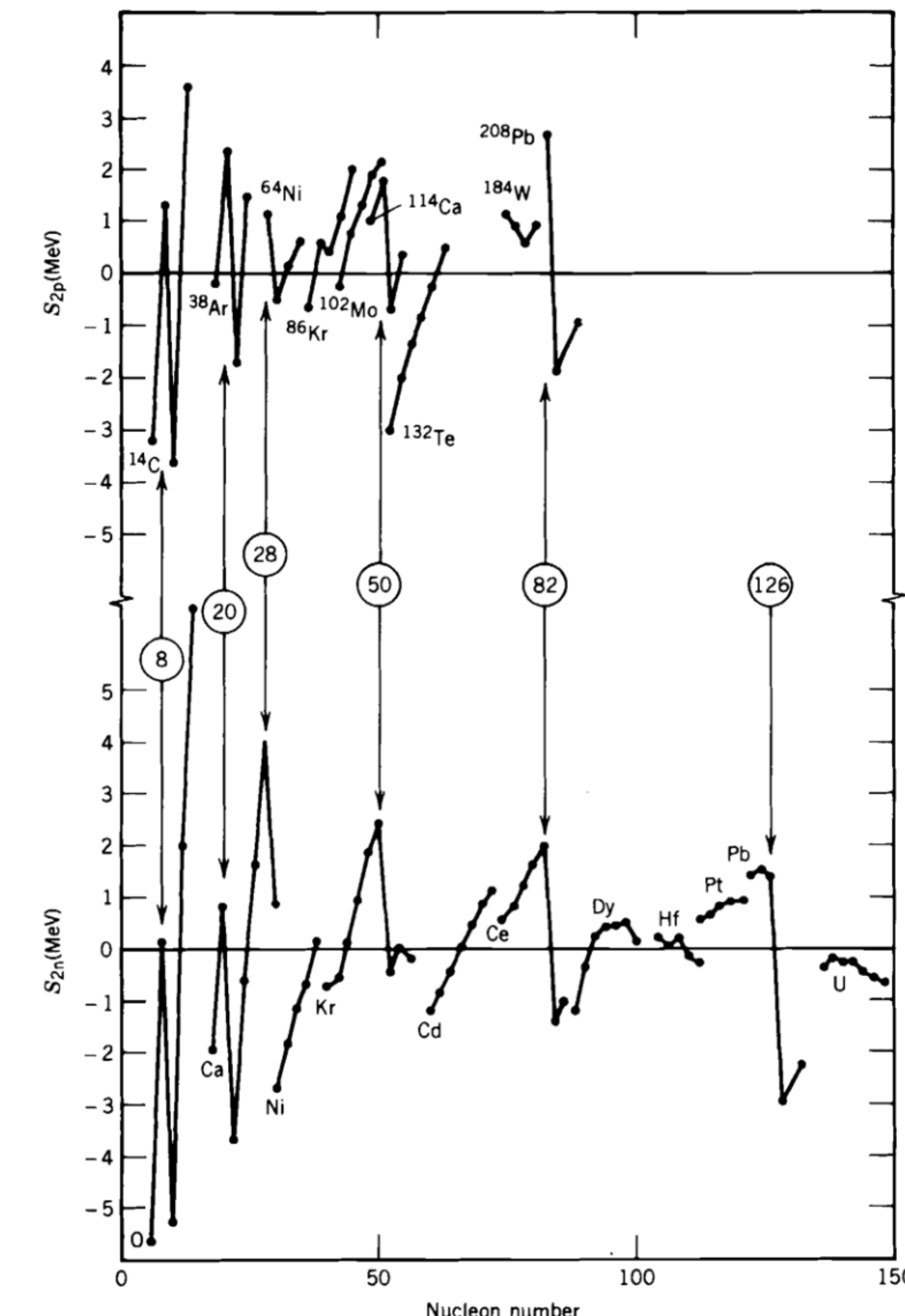


Figure 5.2 (Top) Two-proton separation energies of sequences of isotones (constant N). The lowest Z member of each sequence is noted. (Bottom) Two-neutron separation energies of sequences of isotopes. The sudden changes at the indicated “magic numbers” are apparent. The data plotted are differences between the measured values and the predictions of the semiempirical mass formula. Measured values are from the 1977 atomic mass tables (A. H. Wapstra and K. Bos, *Atomic Data and Nuclear Data Tables* 19, 215 (1977)).

Shell model

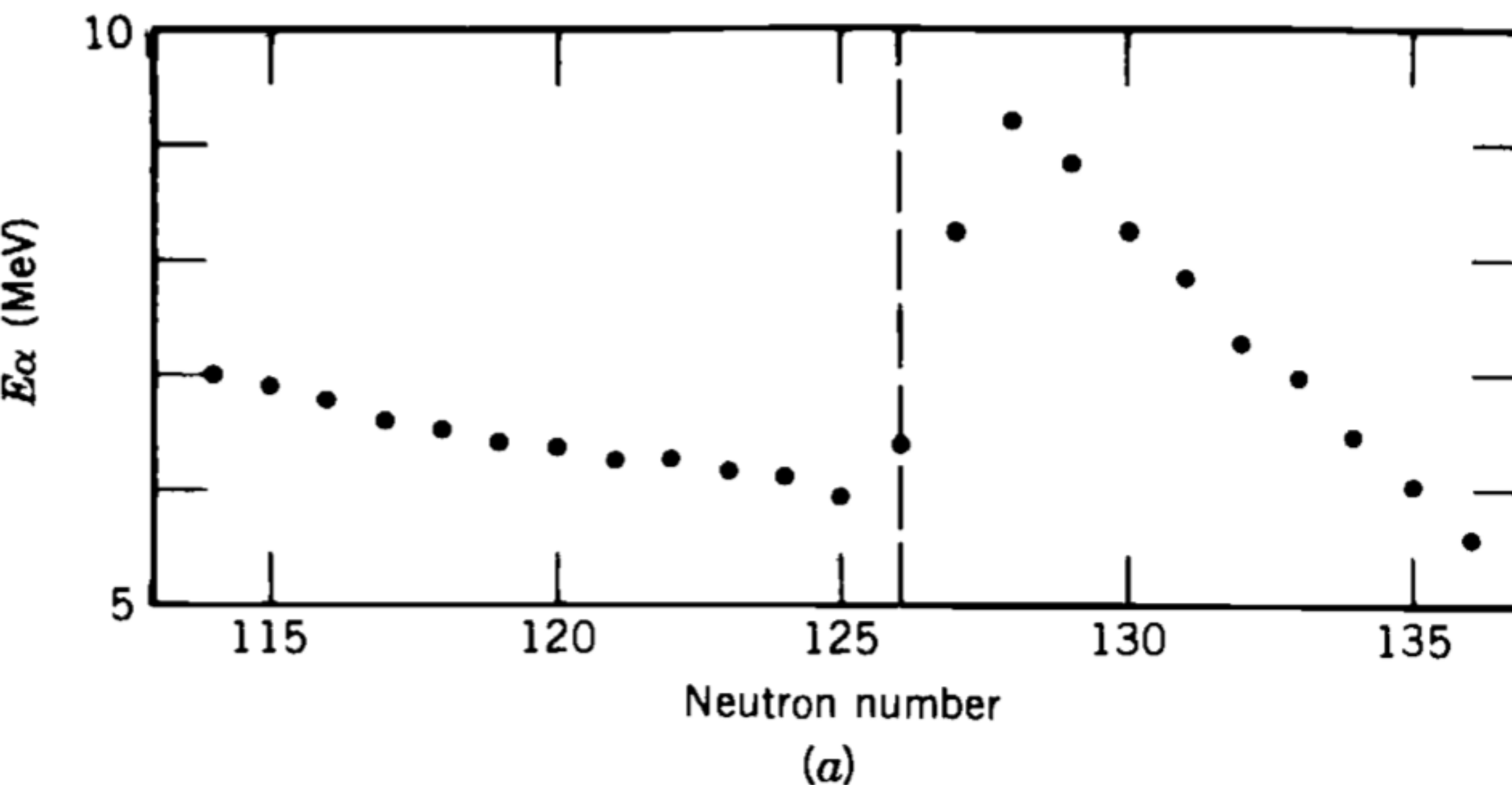
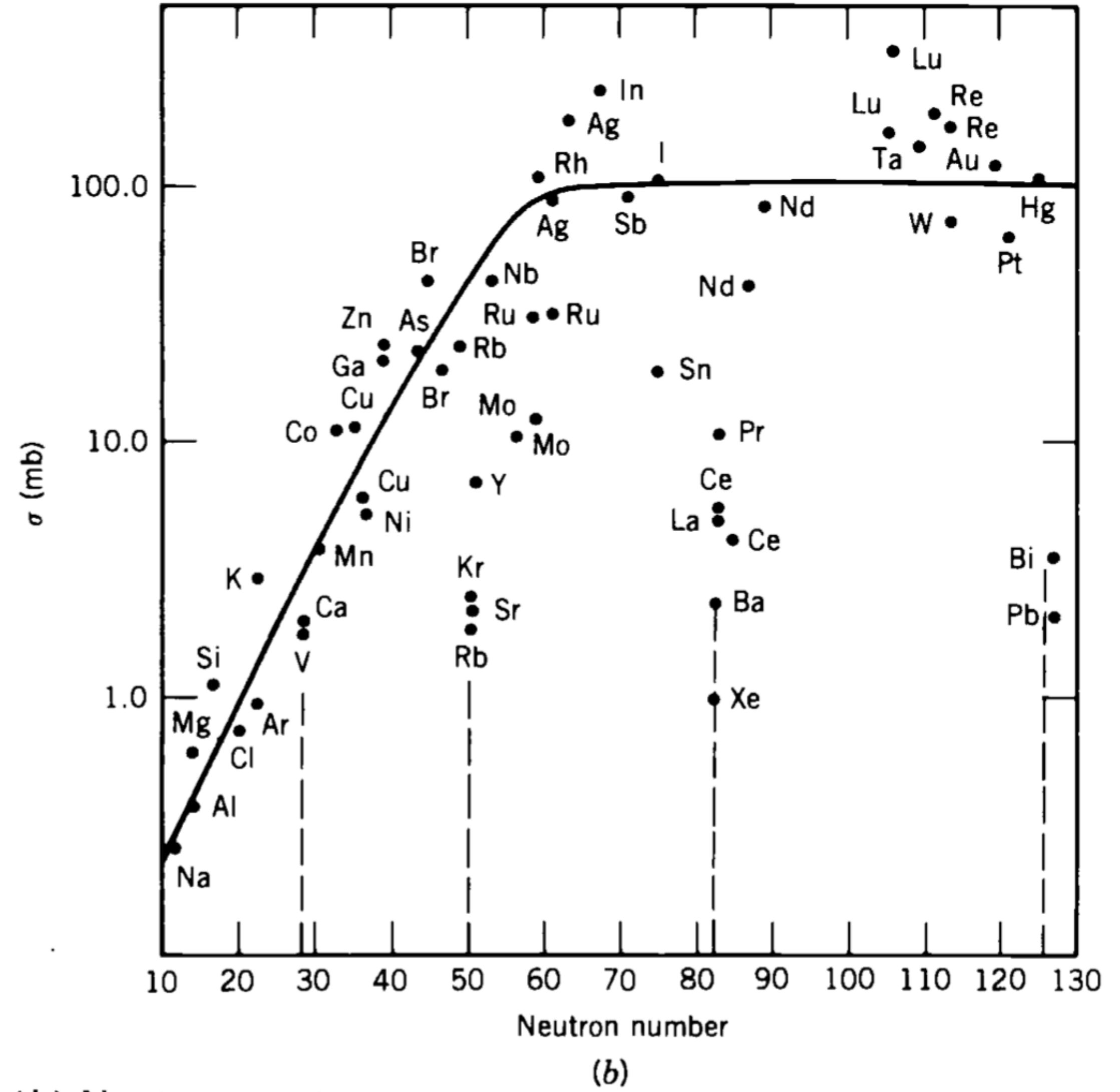


Figure 5.3 Additional evidence for nuclear shell structure. (a) Energies of α particles emitted by isotopes of Rn. Note the sudden increase when the *daughter* has $N = 126$ (i.e., when the parent has $N = 128$). If the daughter nucleus is more tightly bound, the α decay is able to carry away more energy. (b) Neutron-capture

Shell model



tightly bound, the α decay is able to carry away more energy. (b) Neutron-capture cross sections of various nuclei. Note the decreases by roughly two orders of magnitude near $N = 50, 82$, and 126 . (c) Change in the nuclear charge radius when

Shell model

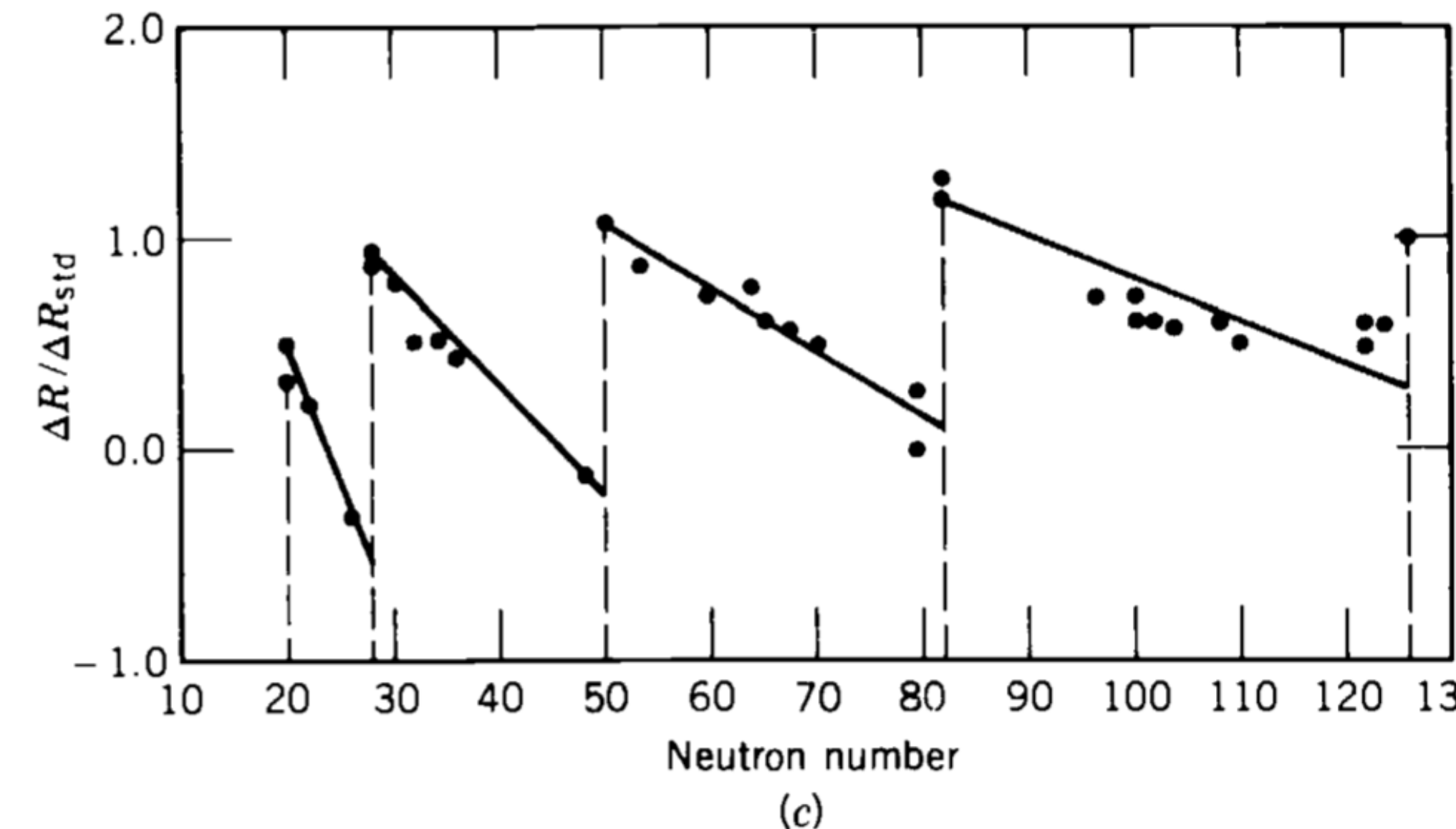


Figure 5.3 Additional evidence for nuclear shell structure. (a) Energies of α particles emitted by isotopes of Rn. Note the sudden increase when the *daughter* has $N = 126$ (i.e., when the parent has $N = 128$). If the daughter nucleus is more tightly bound, the α decay is able to carry away more energy. (b) Neutron-capture cross sections of various nuclei. Note the decreases by roughly two orders of magnitude near $N = 50, 82$, and 126 . (c) Change in the nuclear charge radius when $\Delta N = 2$. Note the sudden jumps at $20, 28, 50, 82$, and 126 and compare with Figure 5.1. To emphasize the shell effects, the radius difference ΔR has been divided by the standard ΔR expected from the $A^{1/3}$ dependence. From E. B. Shera et al., *Phys. Rev. C* **14**, 731 (1976).

Shell model

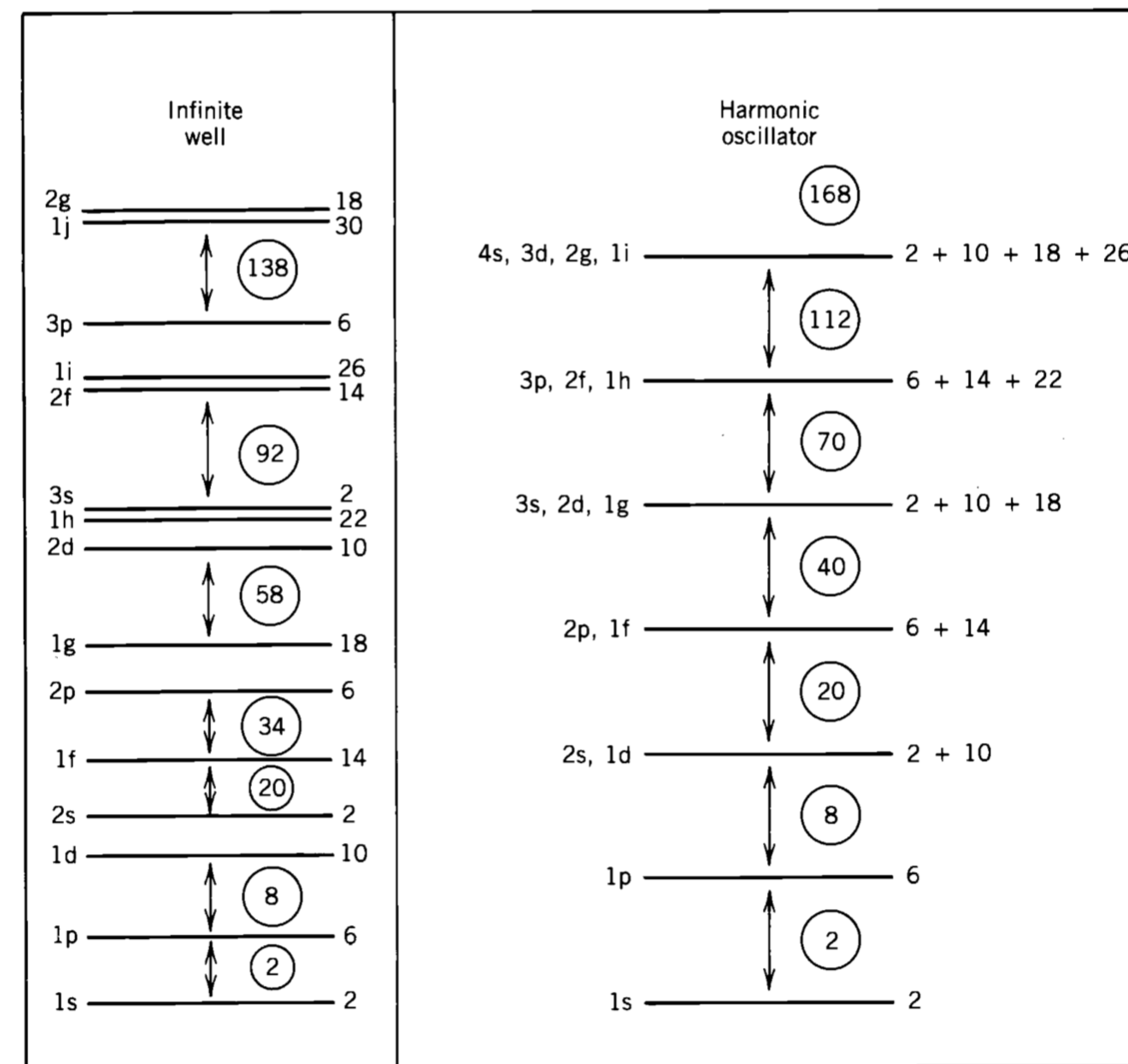


Figure 5.4 Shell structure obtained with infinite well and harmonic oscillator potentials. The capacity of each level is indicated to its right. Large gaps occur between the levels, which we associate with closed shells. The circled numbers indicate the total number of nucleons at each shell closure.

Potential

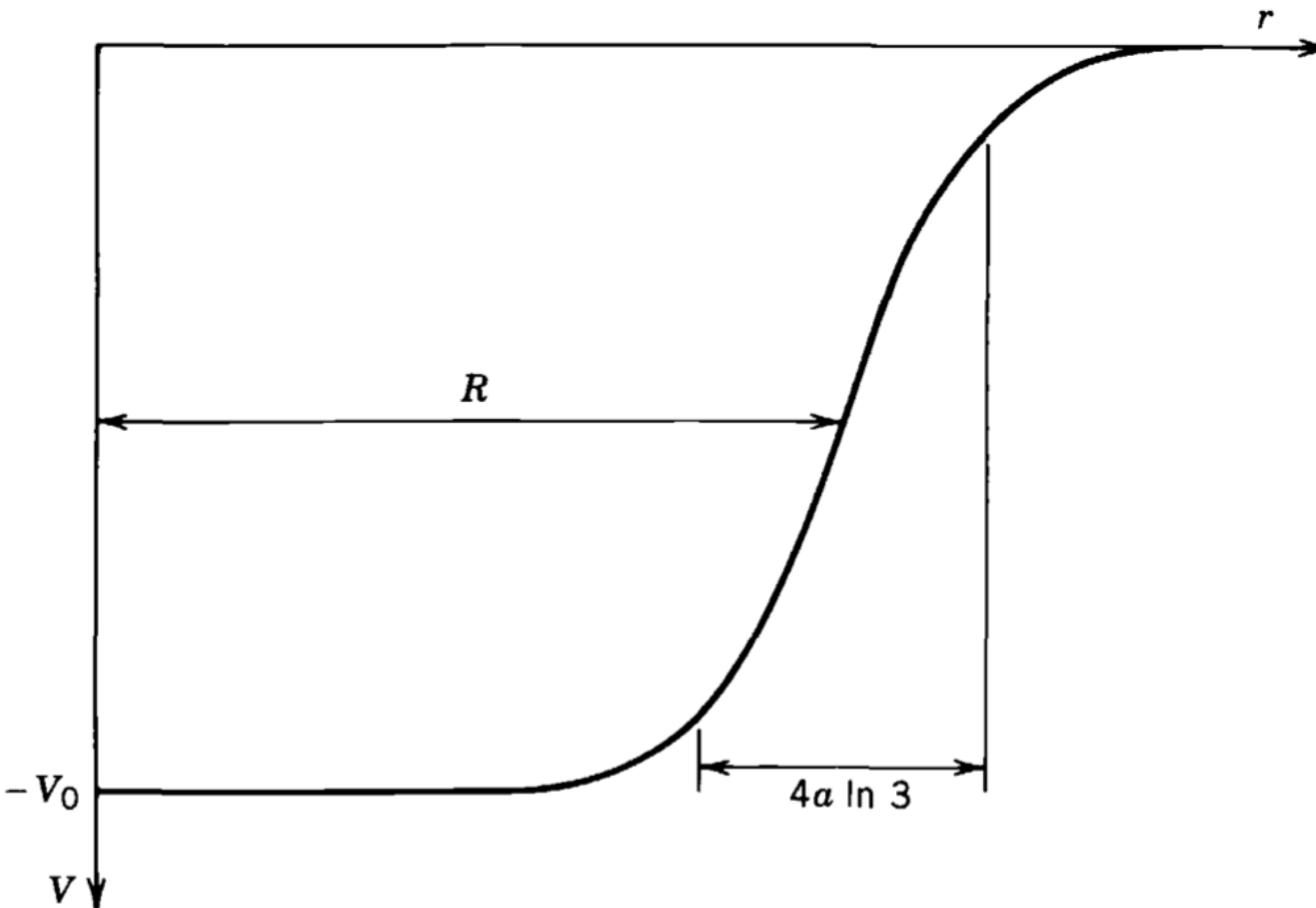


Figure 5.5 A realistic form for the shell-model potential. The “skin thickness” $4a \ln 3$ is the distance over which the potential changes from $0.9V_0$ to $0.1V_0$.

Shell model

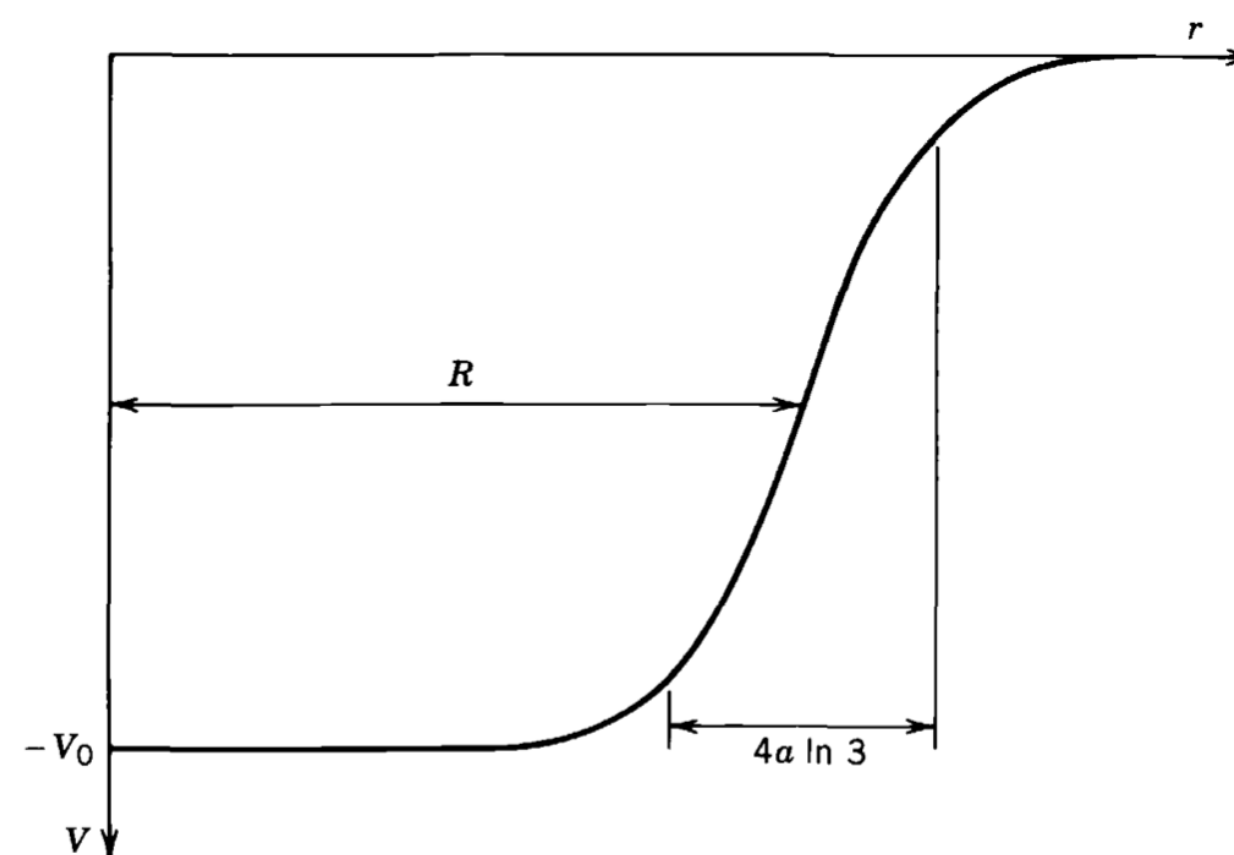


Figure 5.5 A realistic form for the shell-model potential. The “skin thickness” $4a \ln 3$ is the distance over which the potential changes from $0.9V_0$ to $0.1V_0$.

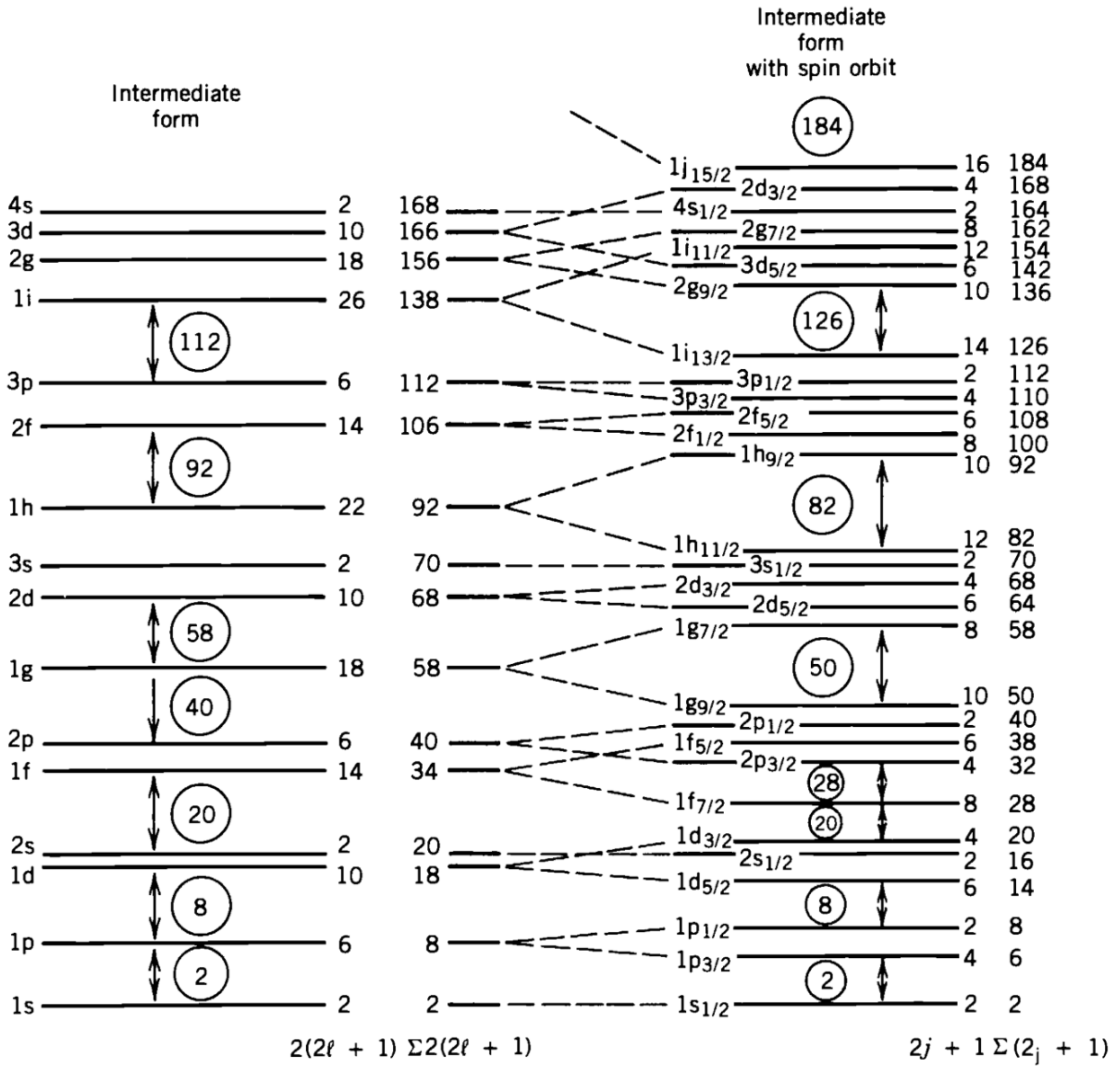


Figure 5.6 At the left are the energy levels calculated with the potential of Figure 5.5. To the right of each level are shown its capacity and the cumulative number of nucleons up to that level. The right side of the figure shows the effect of the spin-orbit interaction, which splits the levels with $\ell > 0$ into two new levels. The shell effect is quite apparent, and the magic numbers are exactly reproduced.

Shell model

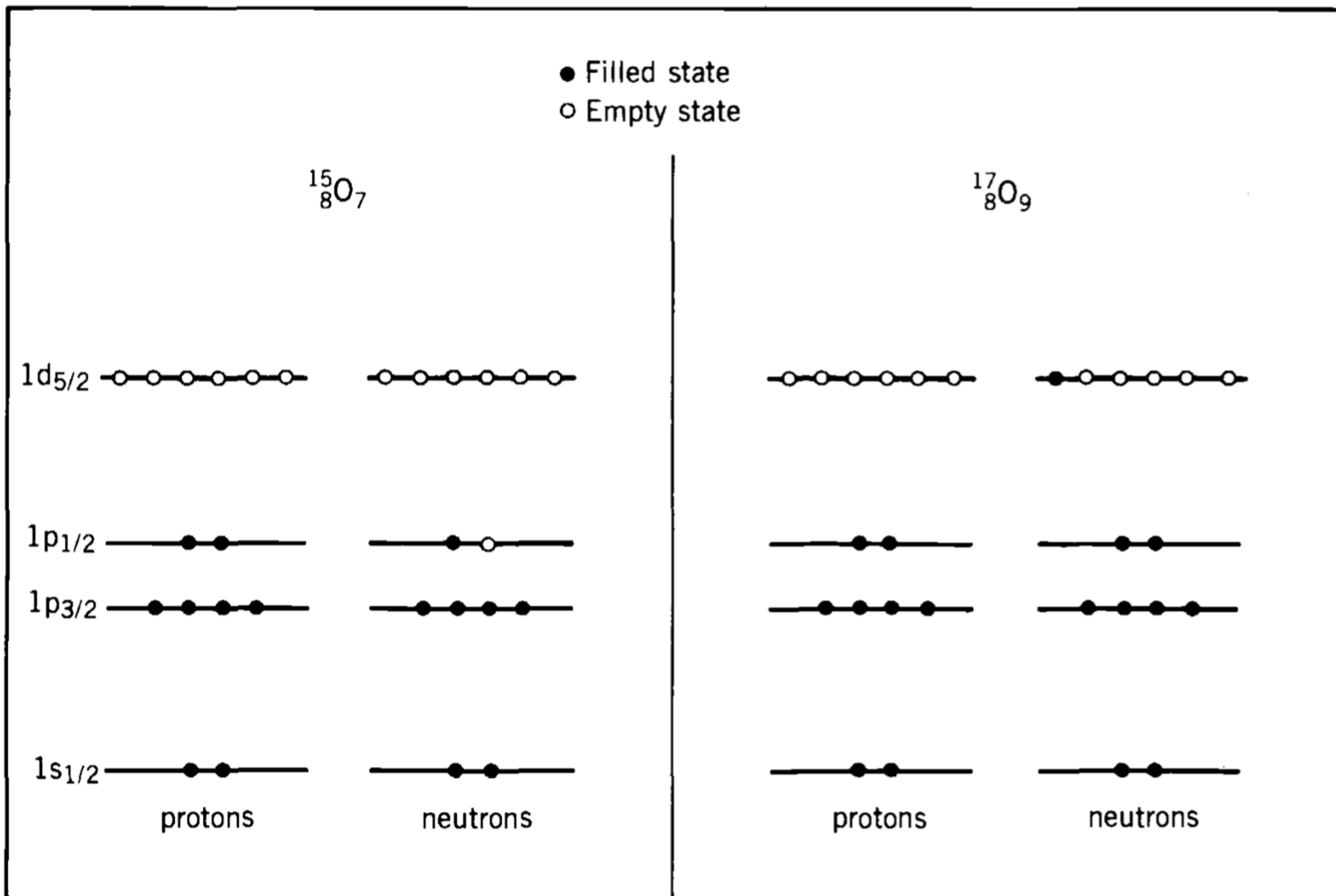


Figure 5.7 The filling of shells in ^{15}O and ^{17}O . The filled proton shells do not contribute to the structure; the properties of the ground state are determined primarily by the odd neutron.

Shell model

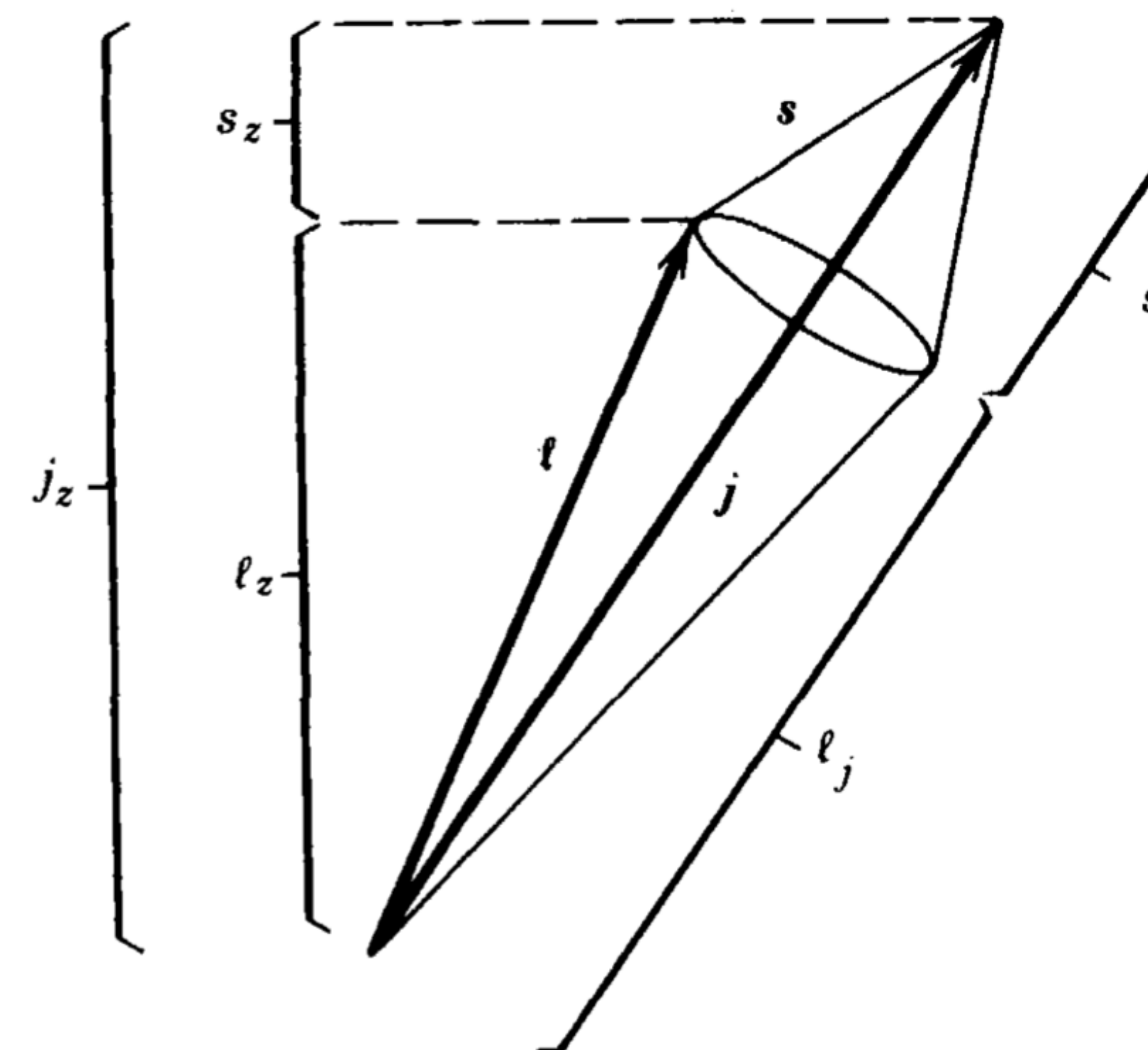


Figure 5.8 As the total angular momentum j precesses about the z axis keeping j_z constant, the vectors ℓ and s precess about j . The components of ℓ and s along j remain constant, but ℓ_z and s_z vary.

Shell model

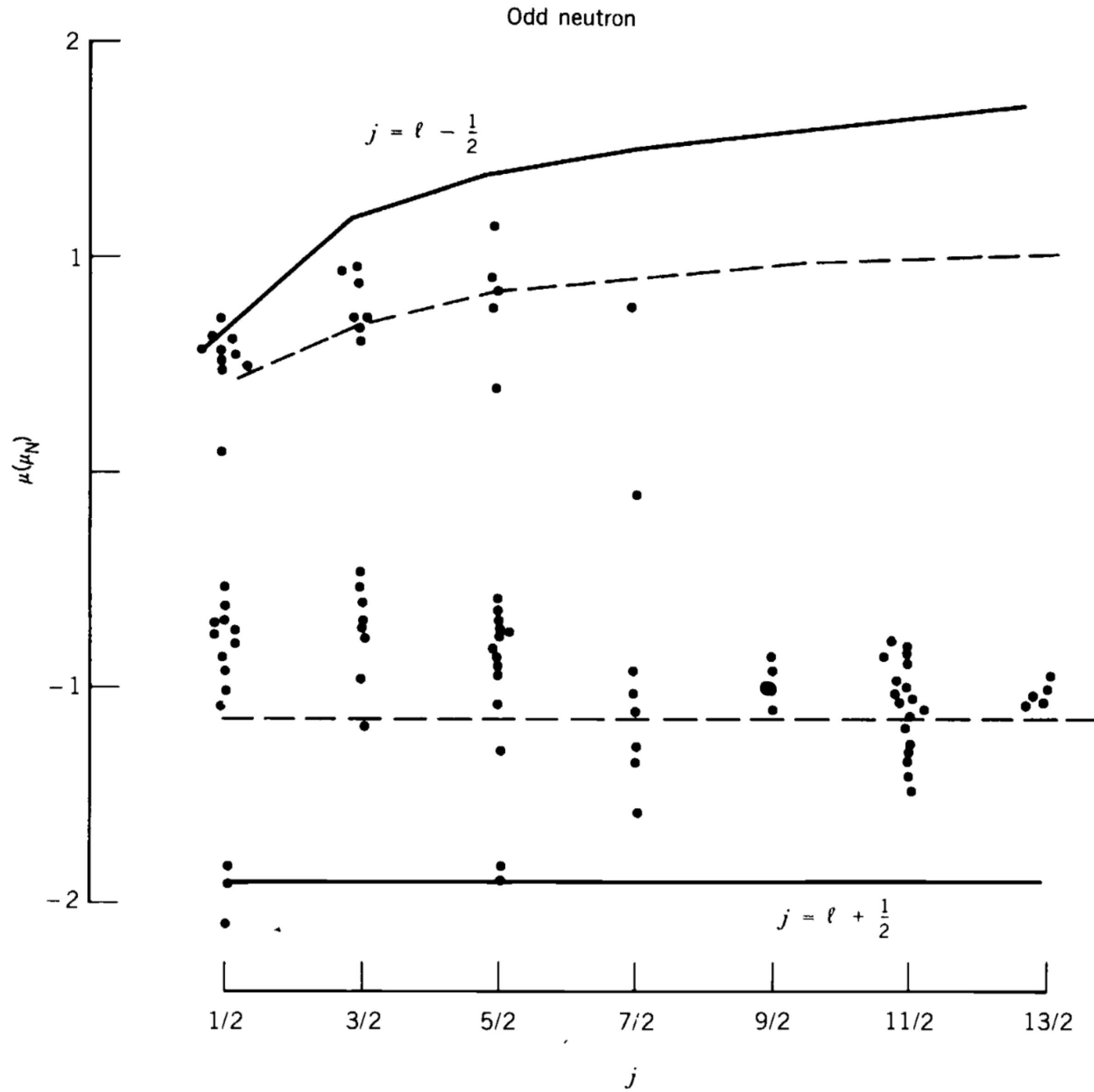


Figure 5.9 Experimental values for the magnetic moments of odd-neutron and odd-proton shell-model nuclei. The Schmidt lines are shown as solid for $g_s = g_s(\text{free})$ and dashed for $g_s = 0.6g_s(\text{free})$.

Shell model

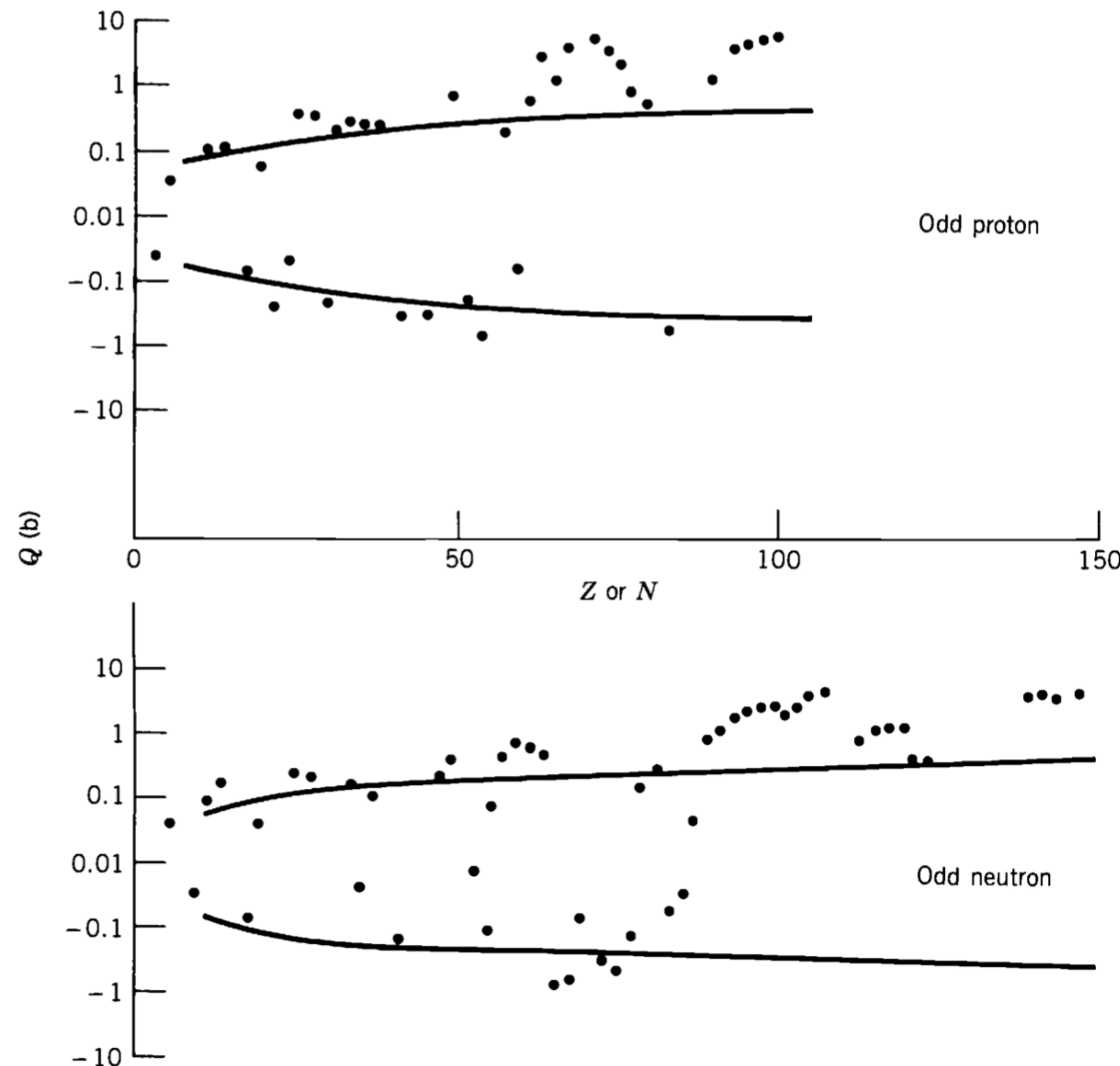


Figure 5.10 Experimental values of electric quadrupole moments of odd-neutron and odd-proton nuclei. The solid lines show the limits $Q \sim \langle r^2 \rangle$ expected for shell-model nuclei. The data are within the limits, except for the regions $60 < Z < 80$, $Z > 90$, $90 < N < 120$, and $N > 140$, where the experimental values are more than an order of magnitude larger than predicted by the shell model.

Shell model

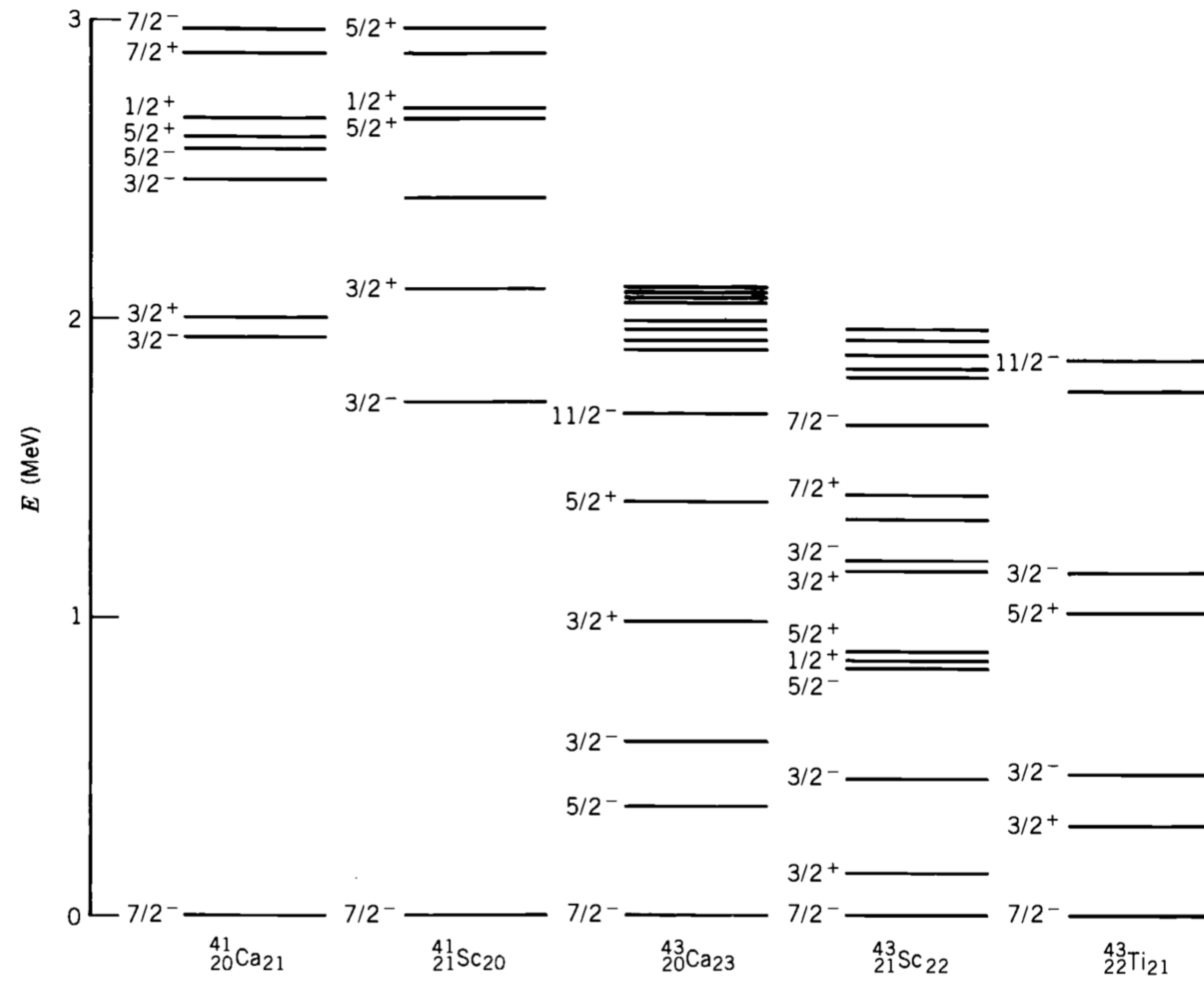


Figure 5.12 Energy levels of nuclei with odd particles in the $1f_{7/2}$ shell.

Shell model

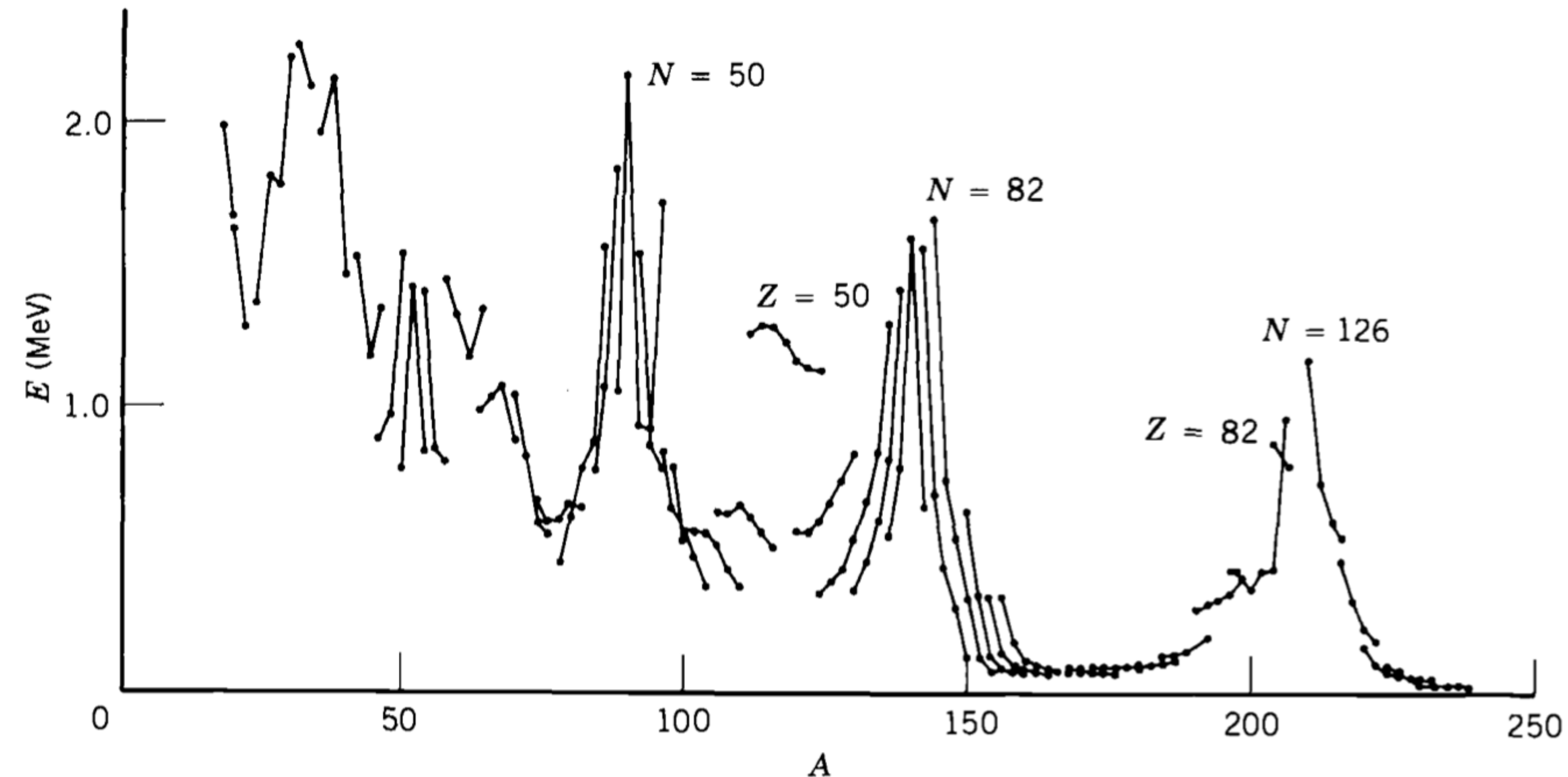


Figure 5.15a Energies of lowest 2^+ states of even- Z , even- N nuclei. The lines connect sequences of isotopes.

Shell model

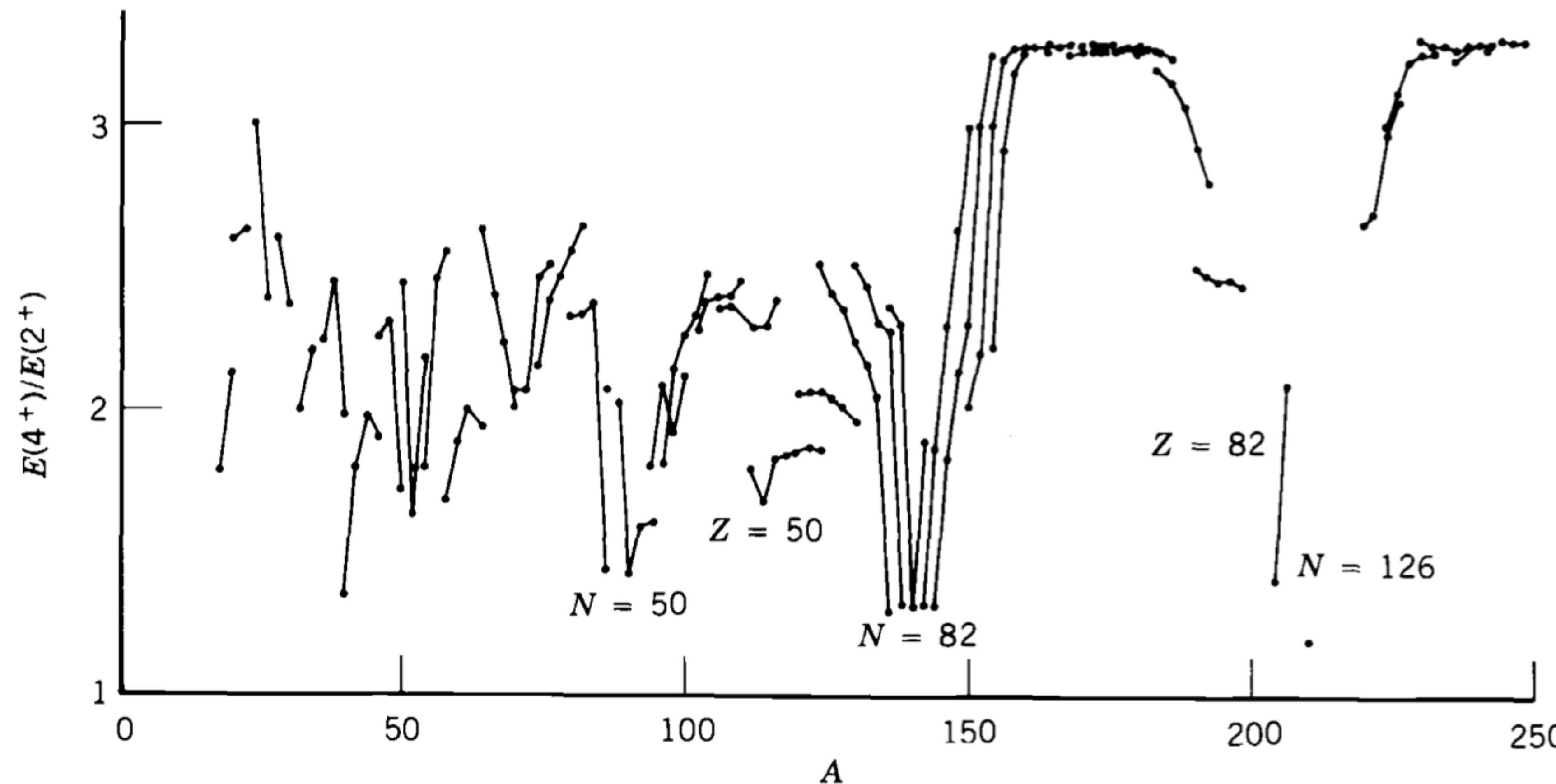


Figure 5.15b The ratio $E(4^+)/E(2^+)$ for the lowest 2^+ and 4^+ states of even- Z , even- N nuclei. The lines connect sequences of isotopes.

Shell model

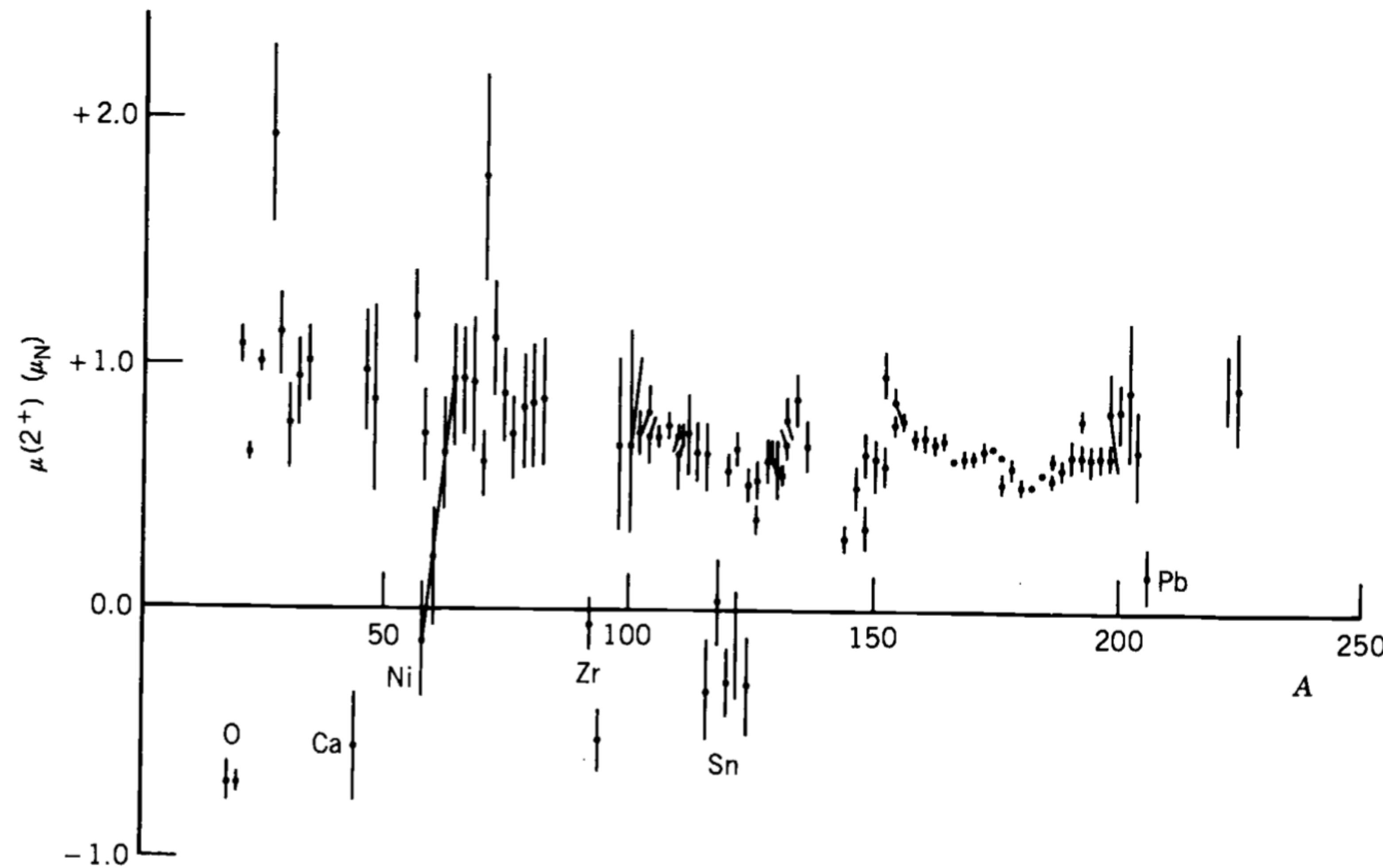


Figure 5.16a Magnetic moments of lowest 2^+ states of even- Z , even- N nuclei. Shell-model nuclei showing noncollective behavior are indicated.

Shell model

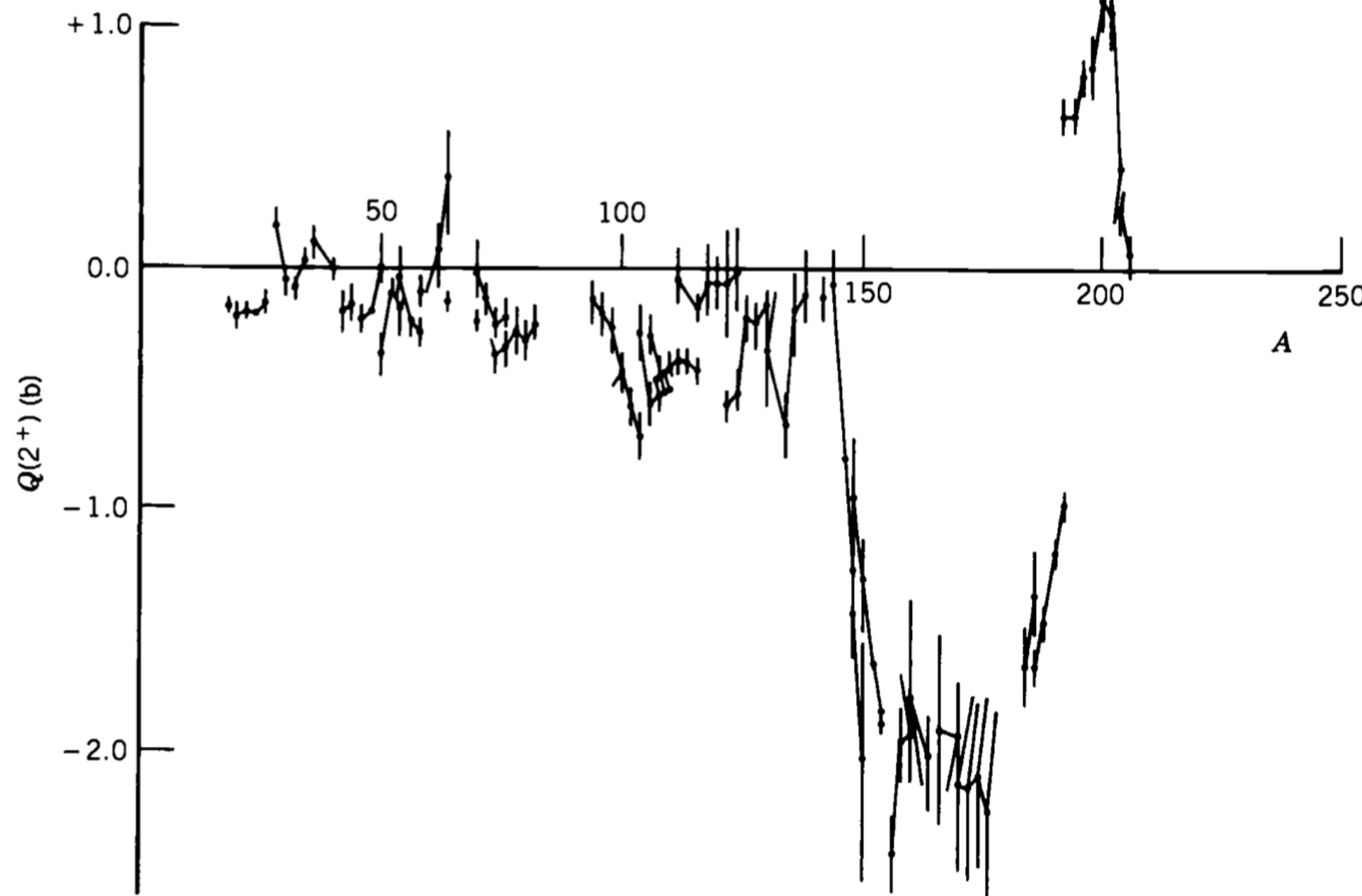


Figure 5.16b Electric quadrupole moments of lowest 2^+ states of even- Z , even- N nuclei. The lines connect sequences of isotopes.

Liquid drop model

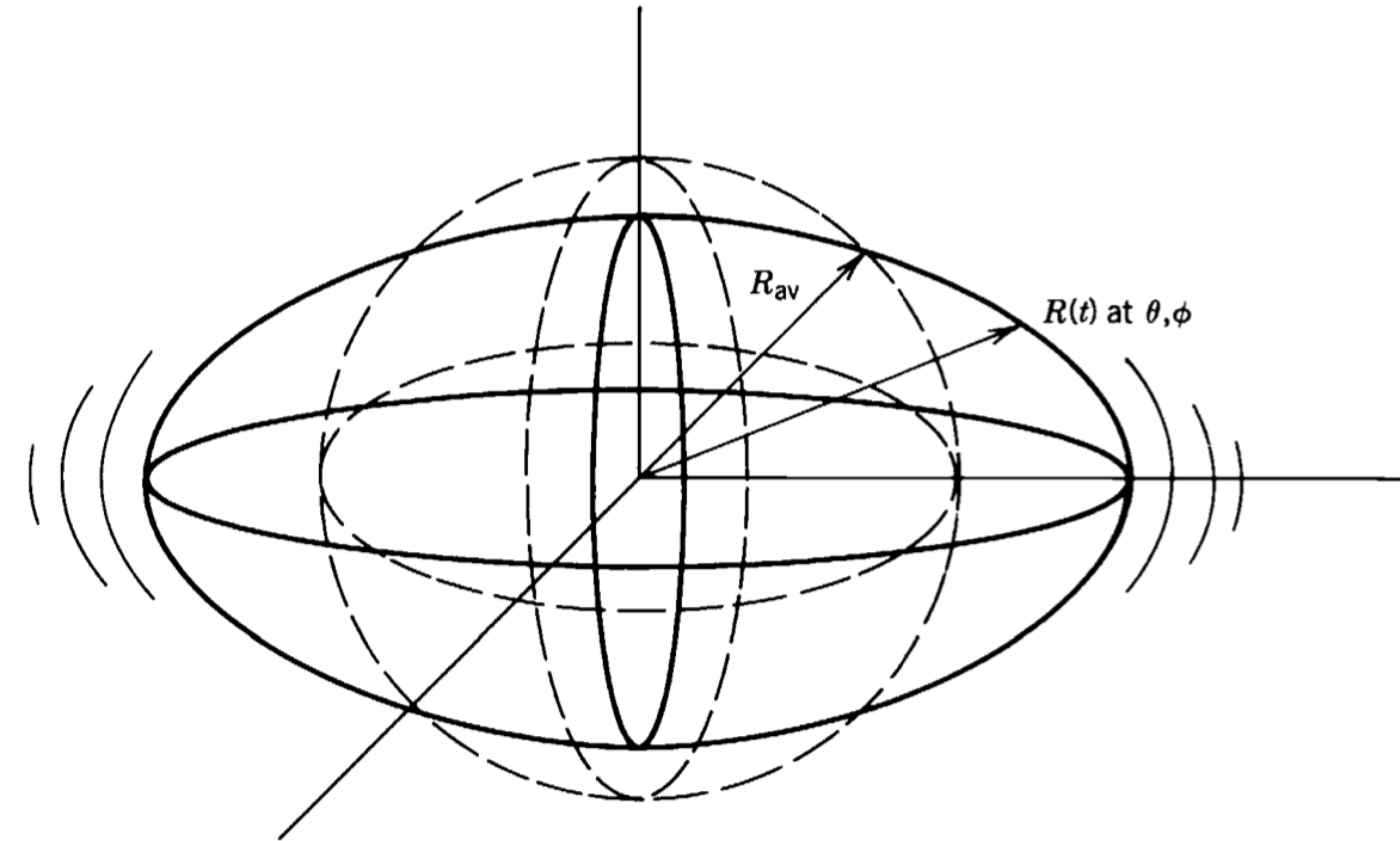


Figure 5.17 A vibrating nucleus with a spherical equilibrium shape. The time-dependent coordinate $R(t)$ locates a point on the surface in the direction θ, ϕ .

Liquid drop model

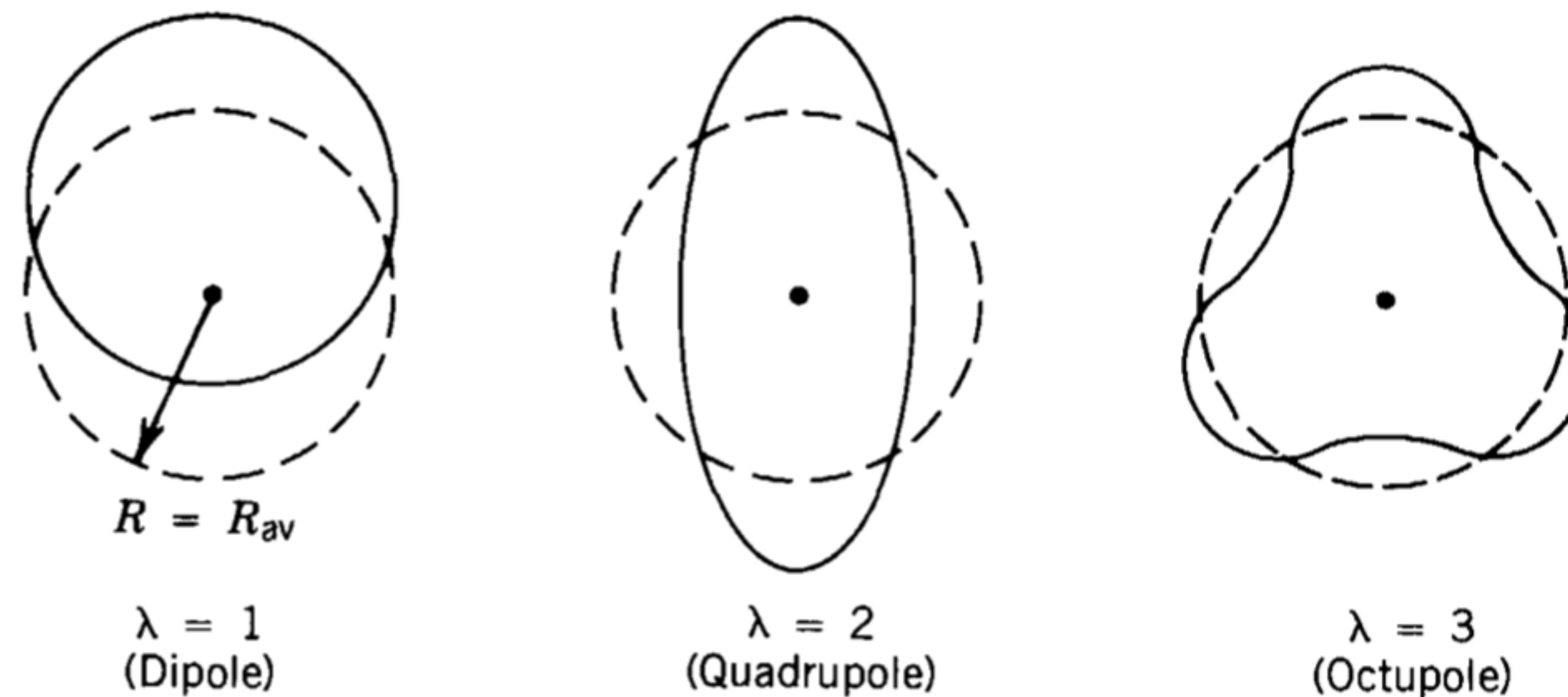


Figure 5.18 The lowest three vibrational modes of a nucleus. The drawings represent a slice through the midplane. The dashed lines show the spherical equilibrium shape and the solid lines show an instantaneous view of the vibrating surface.

Liquid drop model

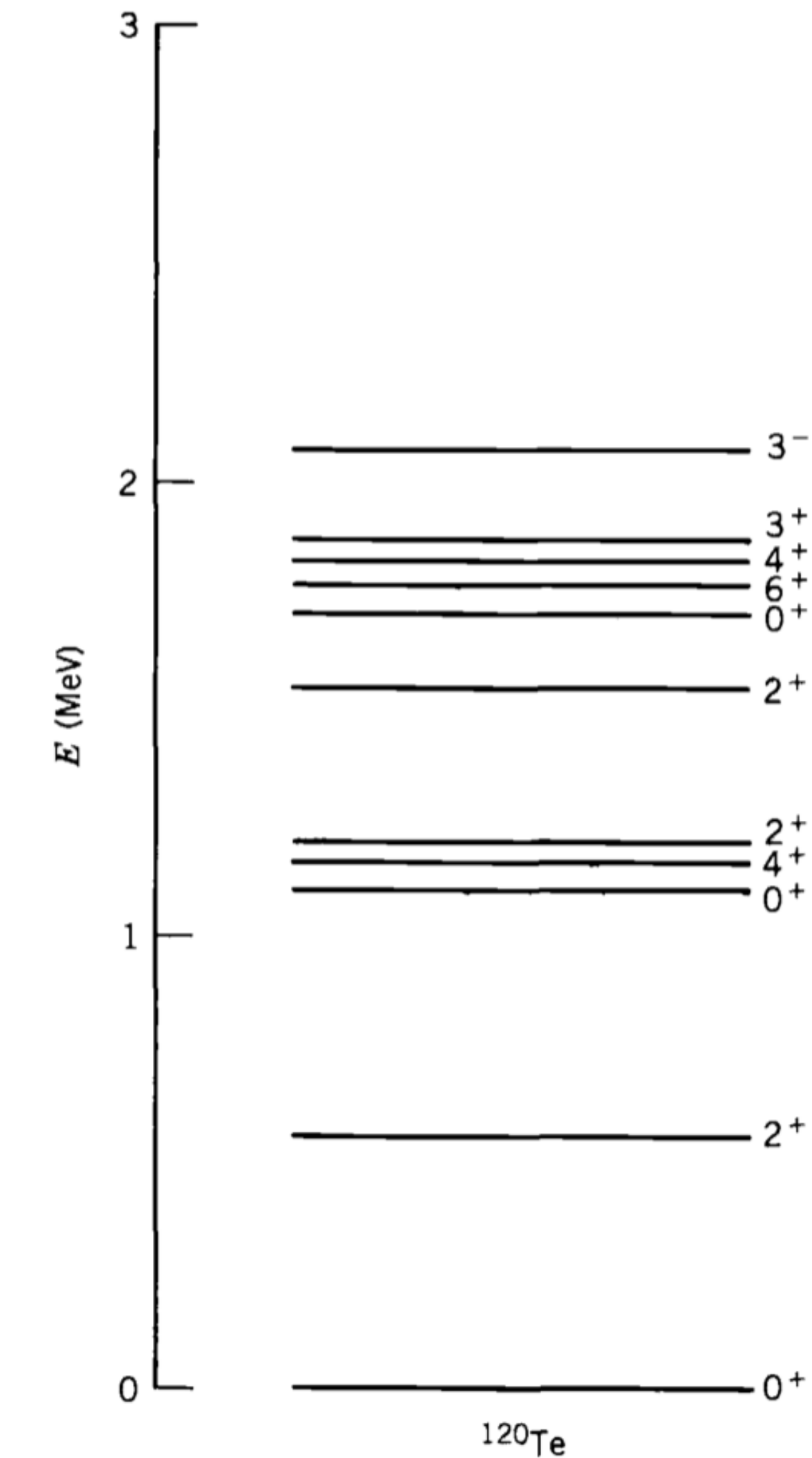


Figure 5.19 The low-lying levels of ^{120}Te . The single quadrupole phonon state (first 2^+), the two-phonon triplet, and the three-phonon quintuplet are obviously seen. The 3^- state presumably is due to the octupole vibration. Above 2 MeV the structure becomes quite complicated, and no vibrational patterns can be seen.

Liquid drop model

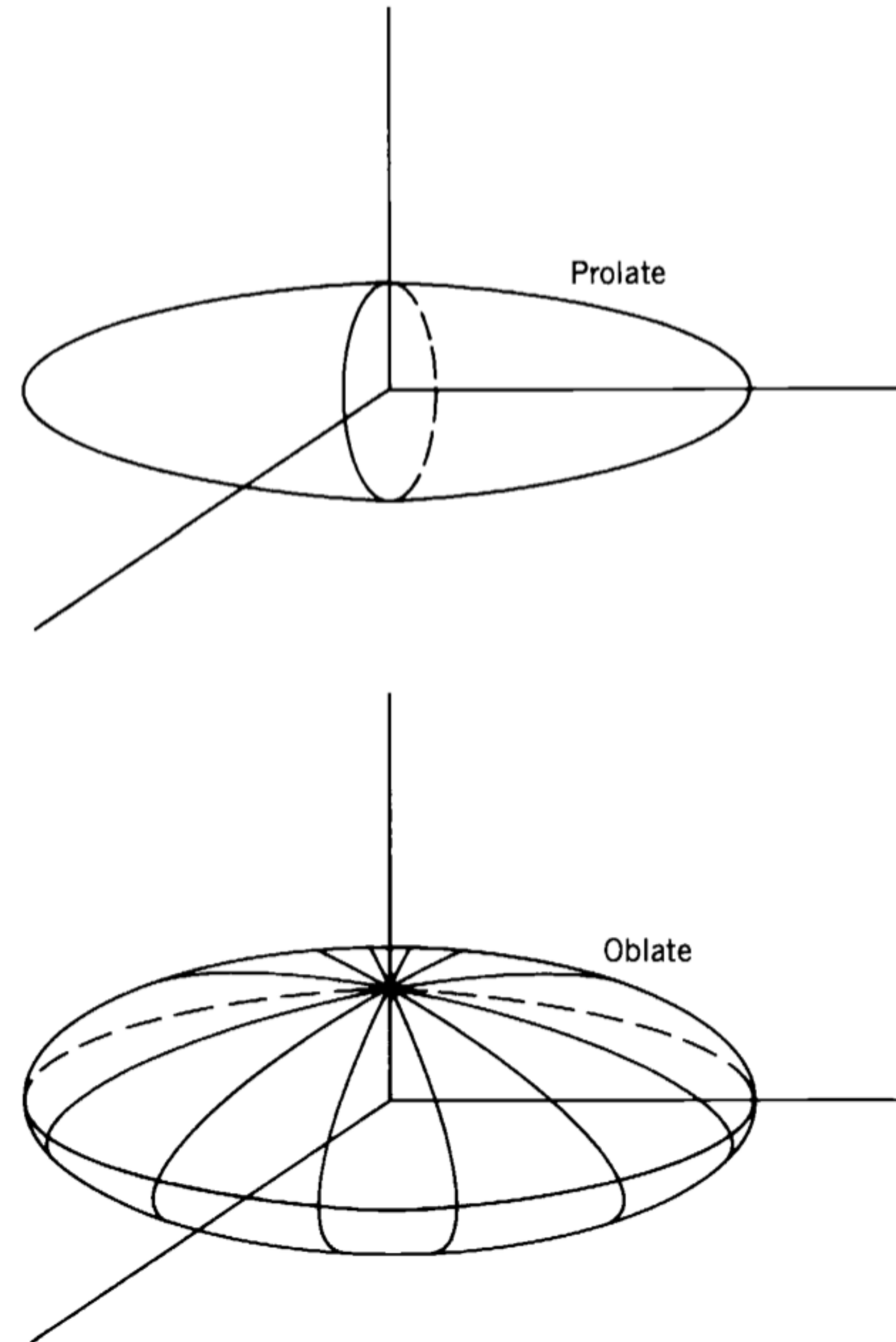


Figure 5.20 Equilibrium shapes of nuclei with permanent deformations. These sketches differ from Figures 5.17 and 5.18 in that these do not represent snapshots of a moving surface at a particular instant of time, but instead show the static shape of the nucleus.

Liquid drop model

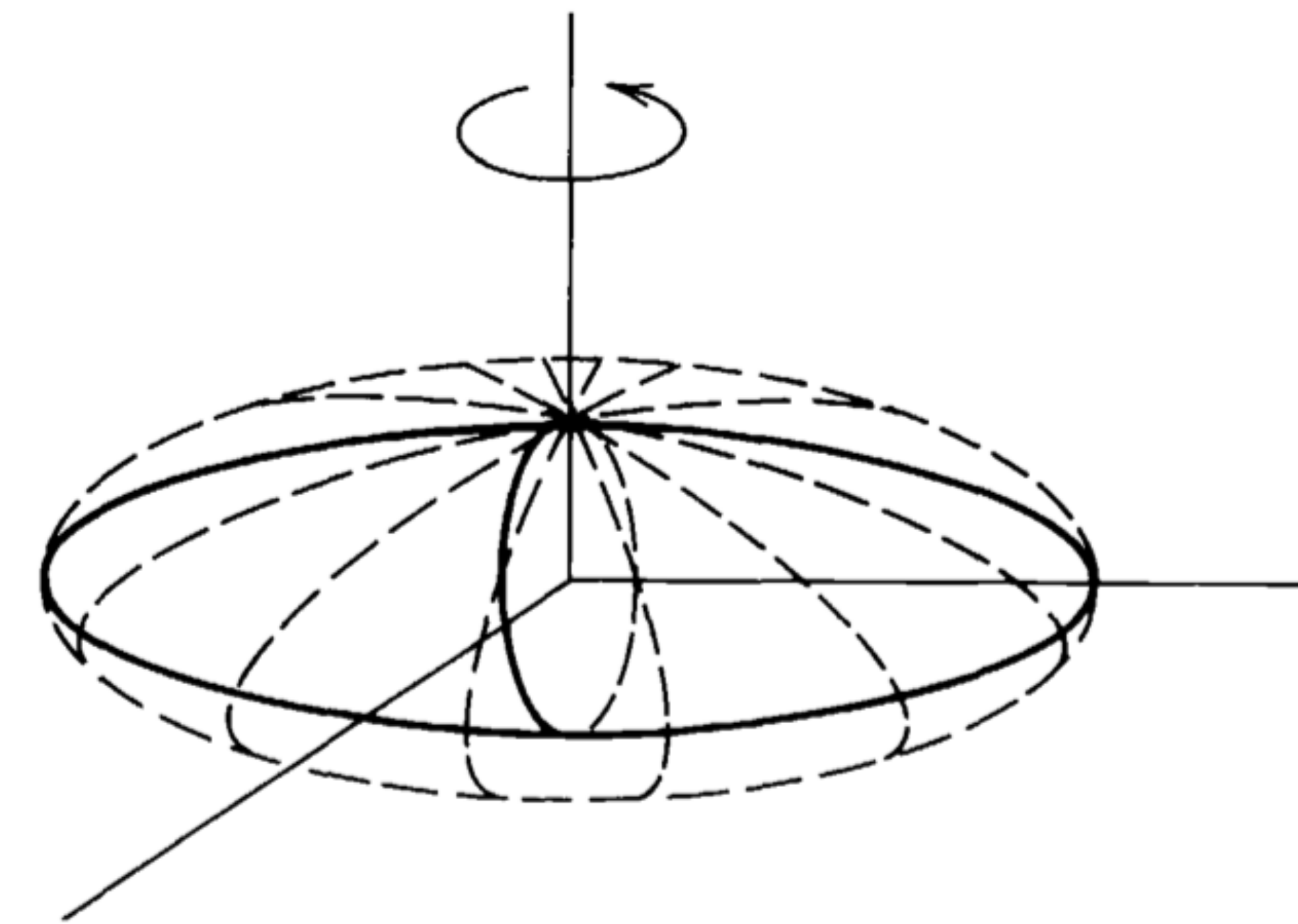


Figure 5.21 Rotating a static prolate distribution about an axis perpendicular to its symmetry axis gives in effect a smeared-out oblate (flattened) distribution.

Liquid drop model

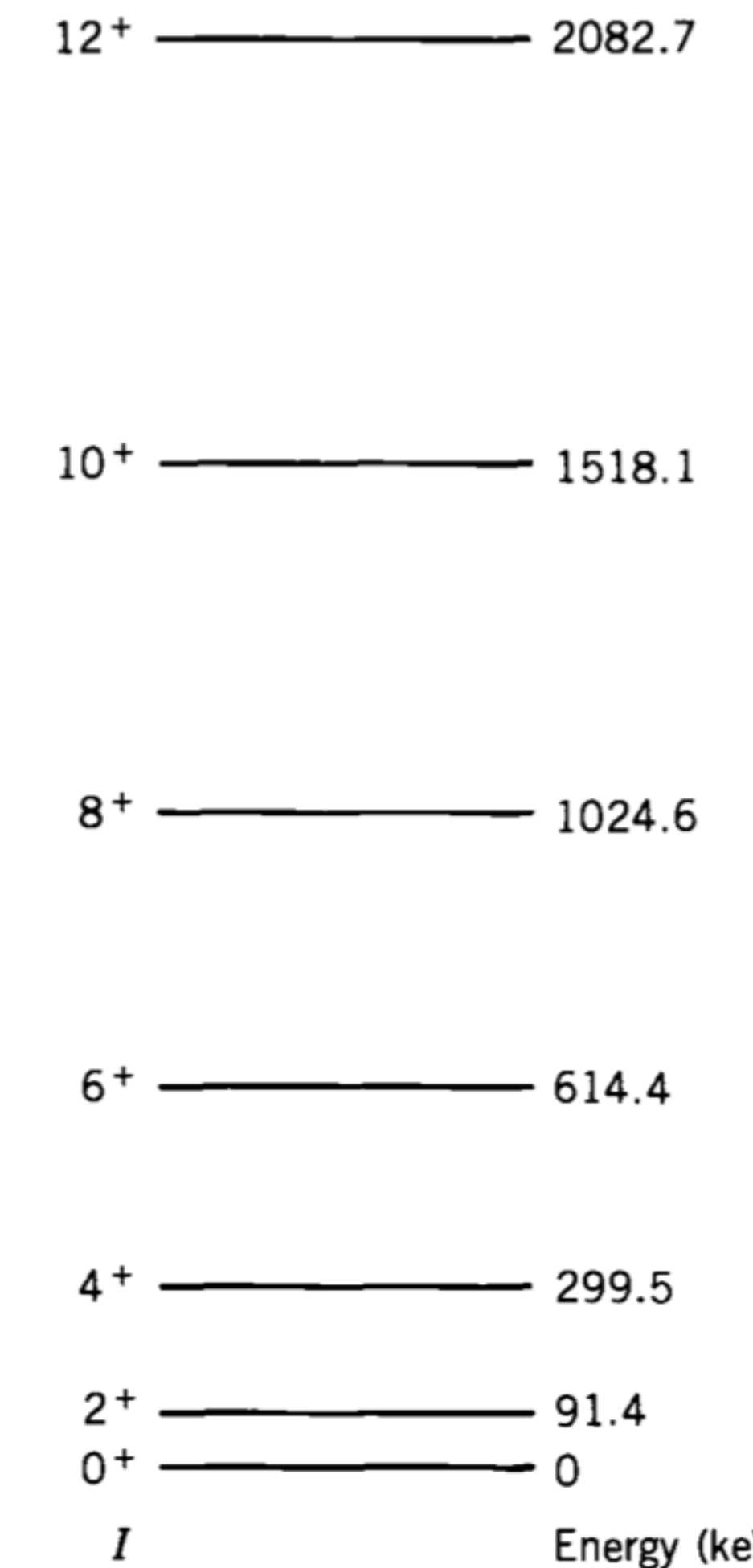


Figure 5.22 The excited states resulting from rotation of the ground state in ^{164}Er .

Liquid drop model

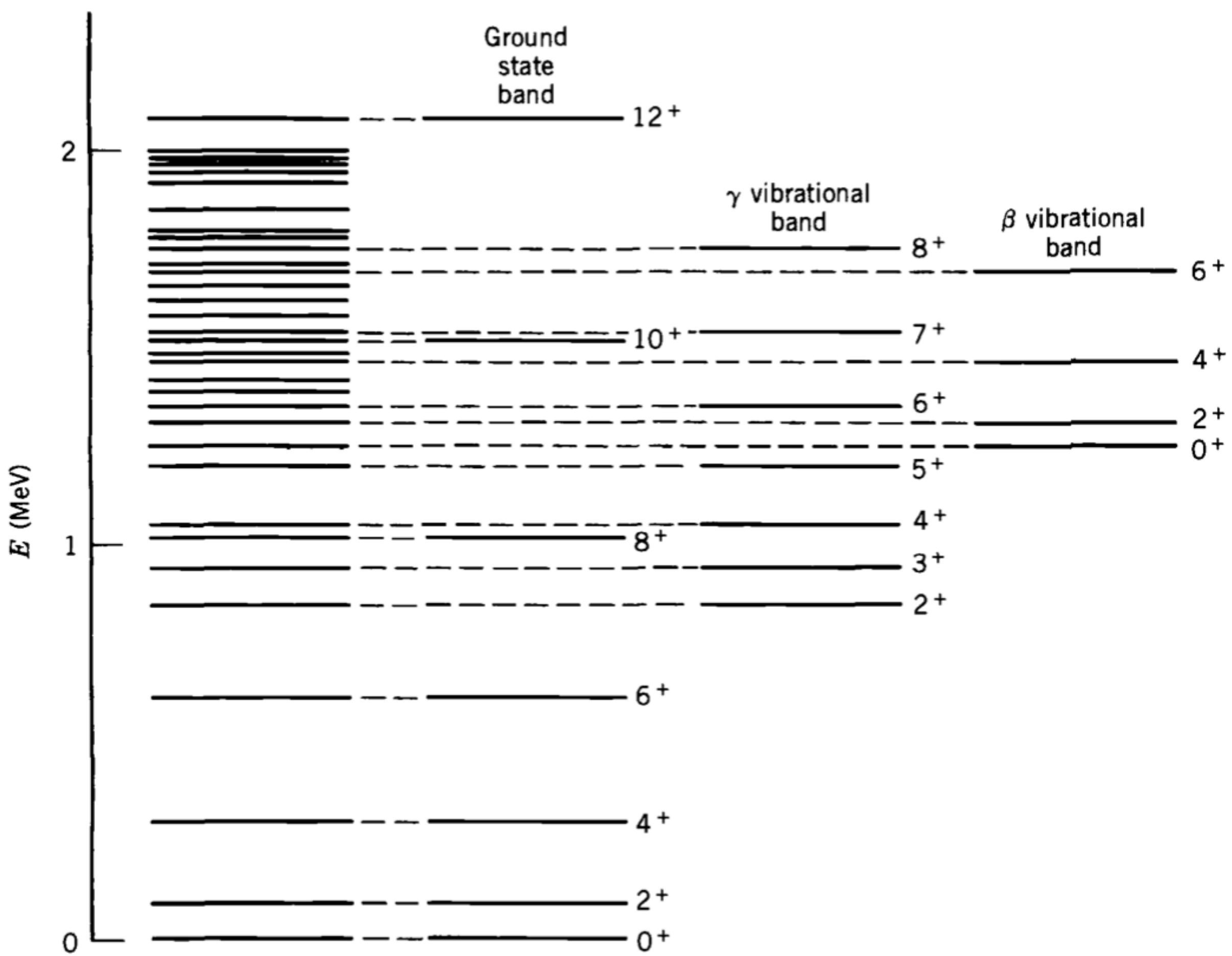


Figure 5.23 The states of ^{164}Er below 2 MeV. Most of the states are identified with three rotational bands: one built on the deformed ground state, a second built on a γ -type vibration (in which the surface vibrates transverse to the symmetry axis), and a third built on a β -type vibration (in which the surface vibrates along the symmetry axis). Many of the other excited states originate from pair-breaking particle excitations and their associated rotational bands.

Liquid drop model

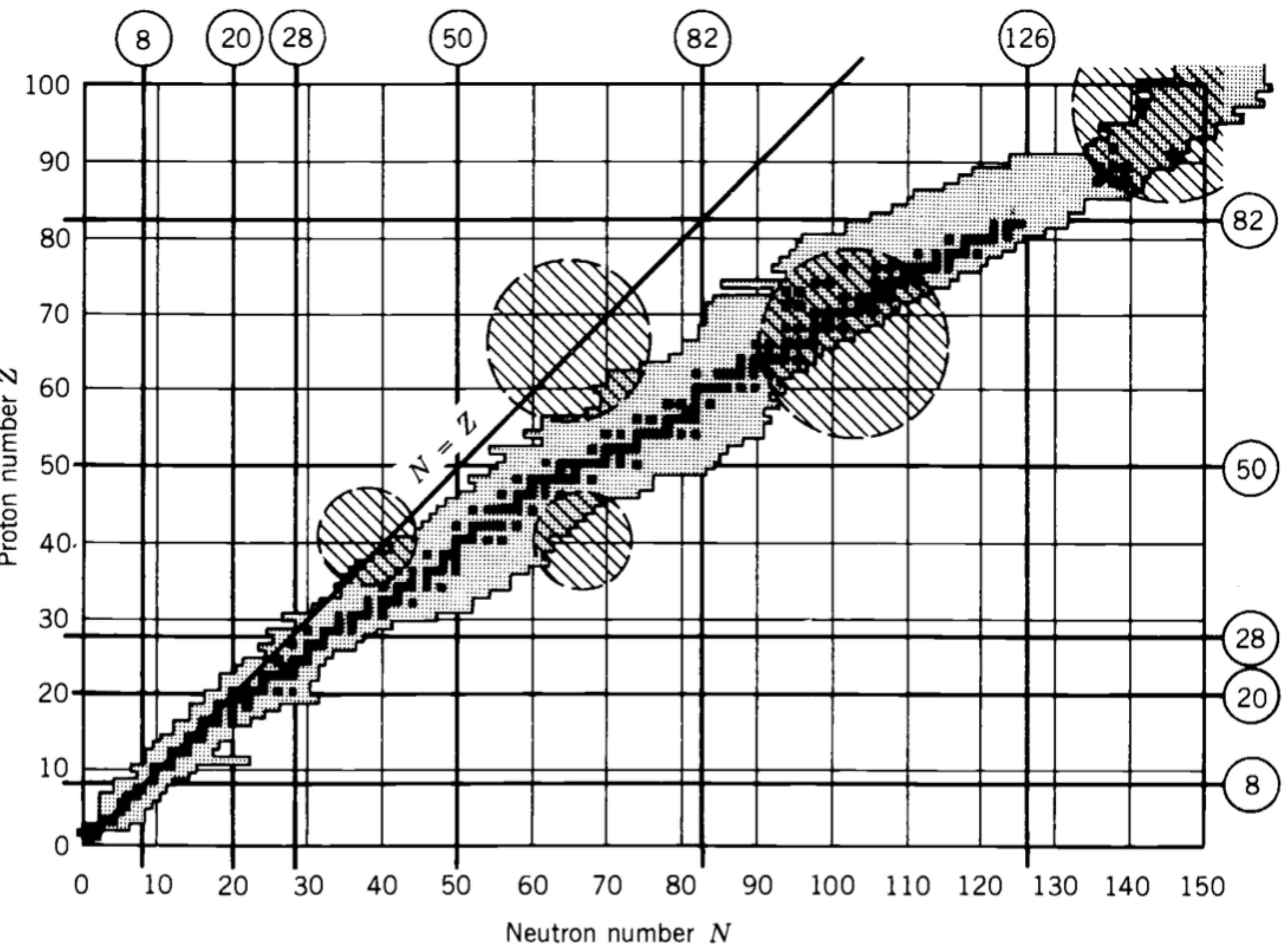


Figure 5.24 The crosshatched areas show the regions far from closed shells where we expect that the cooperative effects of many single-particle shell-model states may combine to produce a permanent nuclear deformation. Such deformed nuclei have been identified in all of the regions where the crosshatched areas overlap the known nuclei.